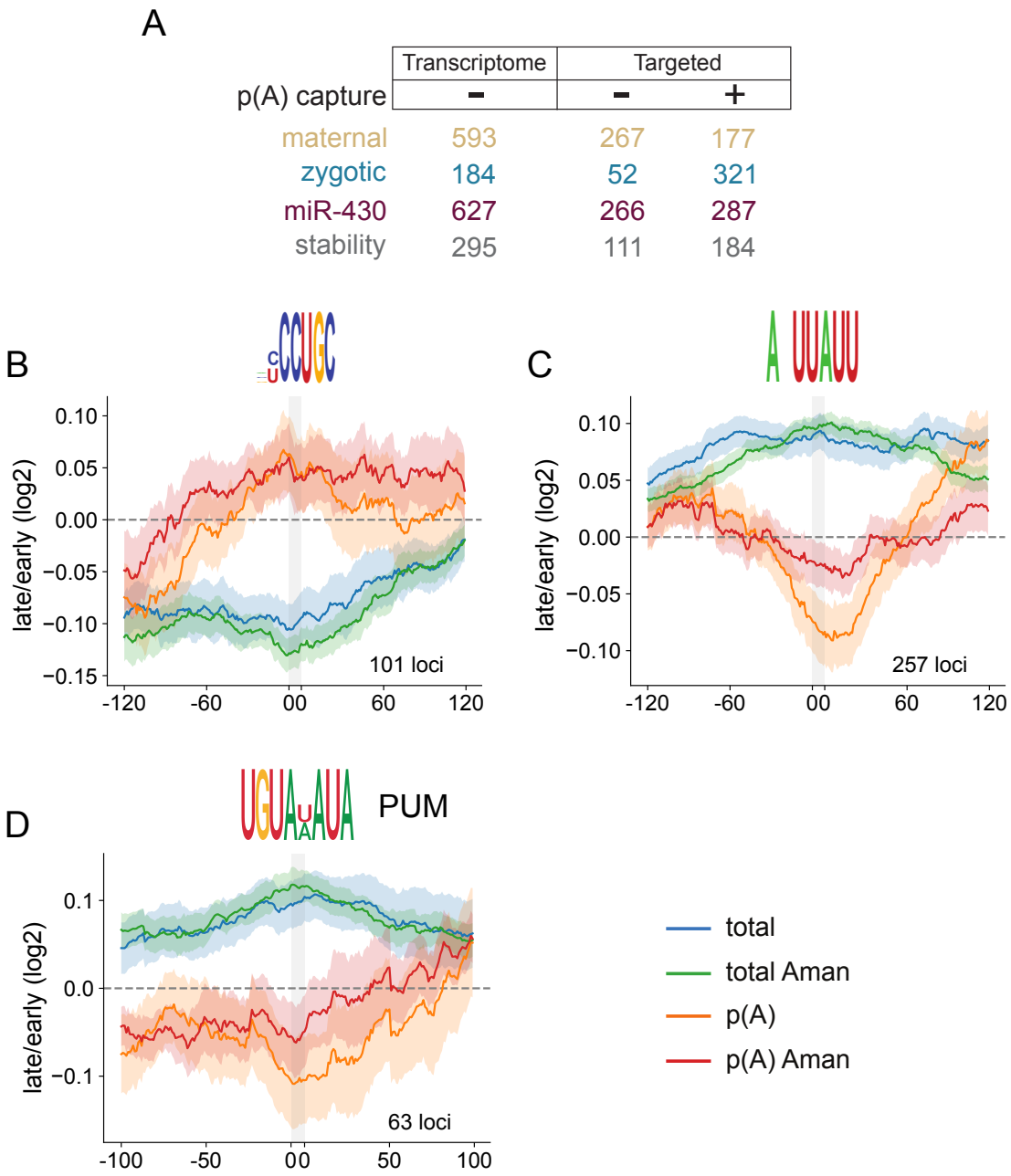

Supplemental Figure S1. (A) Number of regions used for FIRE analysis across transcriptome-based library or targeted library (with/without poly(A) selection) identify sequences under different modes of regulation. (B-D) Motif-centered metaplots for CCUGC (B), ANUUAUU (C), and Pumilio (D) motifs. Targeted RESA libraries coverage ratio were averaged over windows centered on RBP motif (RESA minimum coverage >0.01 CPM). Motif is represented with grey bar. S.E.M. of RESA is shown by shaded outlines.

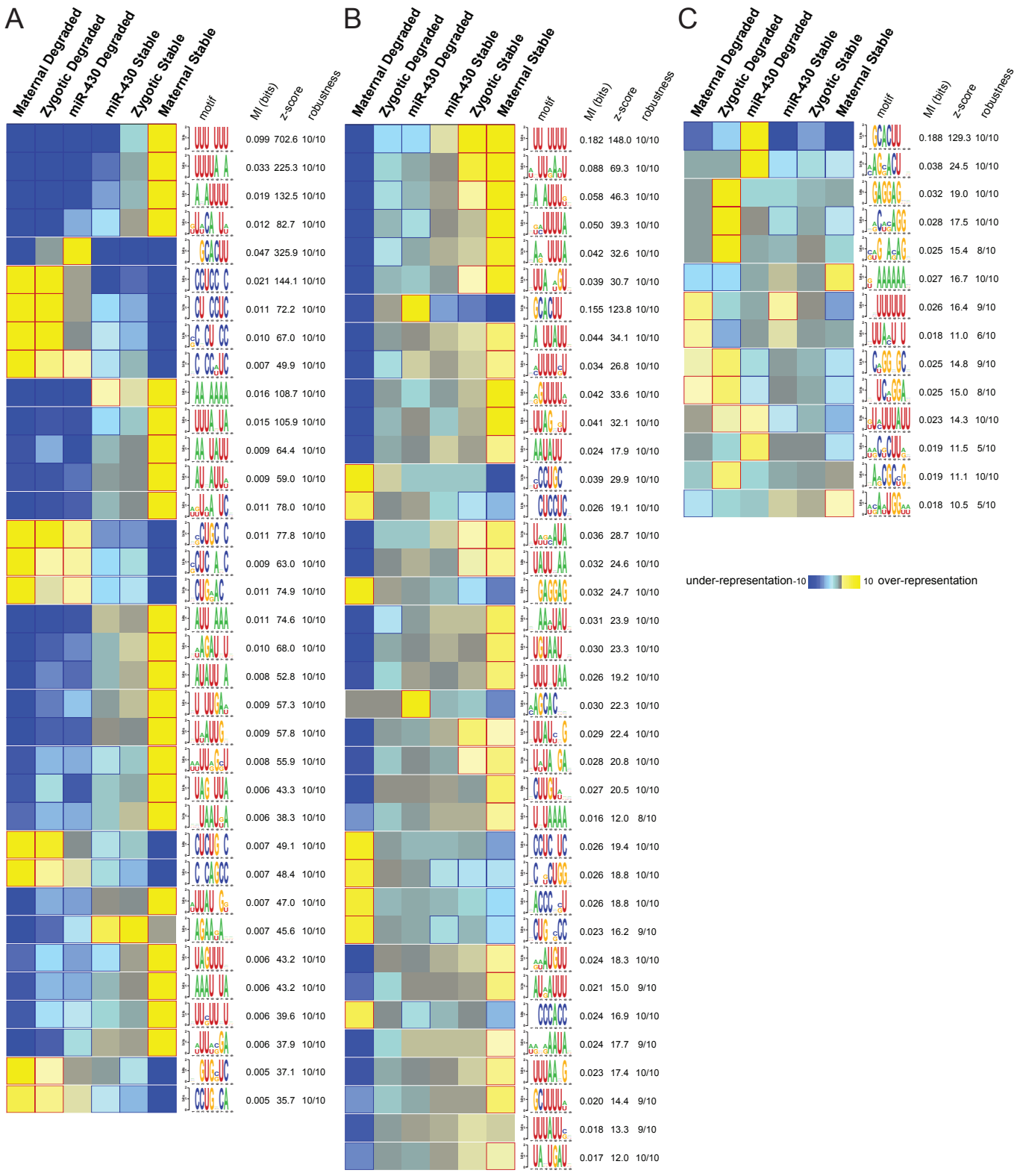

Supplemental Figure S2. Full list of linear motifs discovered by FIRE that were informative of the various modes of regulation across the RESA libraries for (A) the transcriptomic library, (B) the targeted library, and (C) the poly(A) selected targeted library. Shown are each motif primary sequence in a weblogo format, its associated mutual information value, Z-score (estimated using a randomization-based statistical test; Elemento et al, 2007), and its robustness score from a three-fold jackknifing test (Elemento et al, 2007). Yellow entries denote enrichment while blue entries mark significant depletion of a given motif in each corresponding cluster. Z-score cut-off of 20 for the transcriptomic and 10 for the targeted libraries.

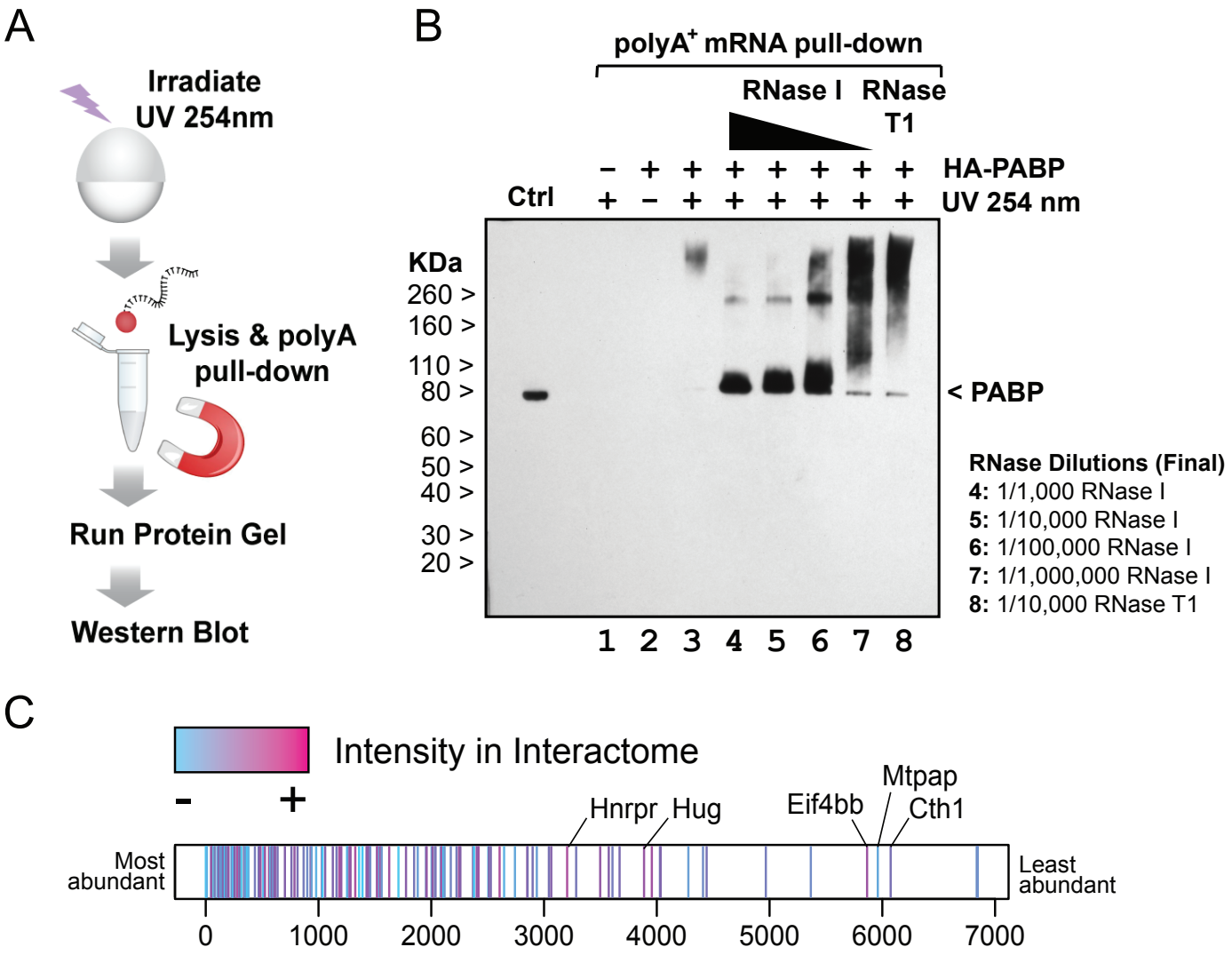

Supplemental Figure S3. (A) Schematic presentation of the experimental procedure for interactome capture (B) Efficiency/specificity of capture after *in vivo* UV crosslinking in embryos was assessed by measuring capture efficiency of an HA-tagged variant of PABP, an abundant protein that binds to the 3' ends of poly(A) transcripts. (C) Interactome capture identifies RBPs from all the range of expression levels. Proteins identified in the input were ranked according to their abundance in the whole-embryo lysate. Proteins identified in the interactome capture were then labeled according to their intensity in the interactome capture. Although overall abundance of individual proteins (input) generally correlated with capture efficiency, several of the most highly captured proteins were lowly expressed.

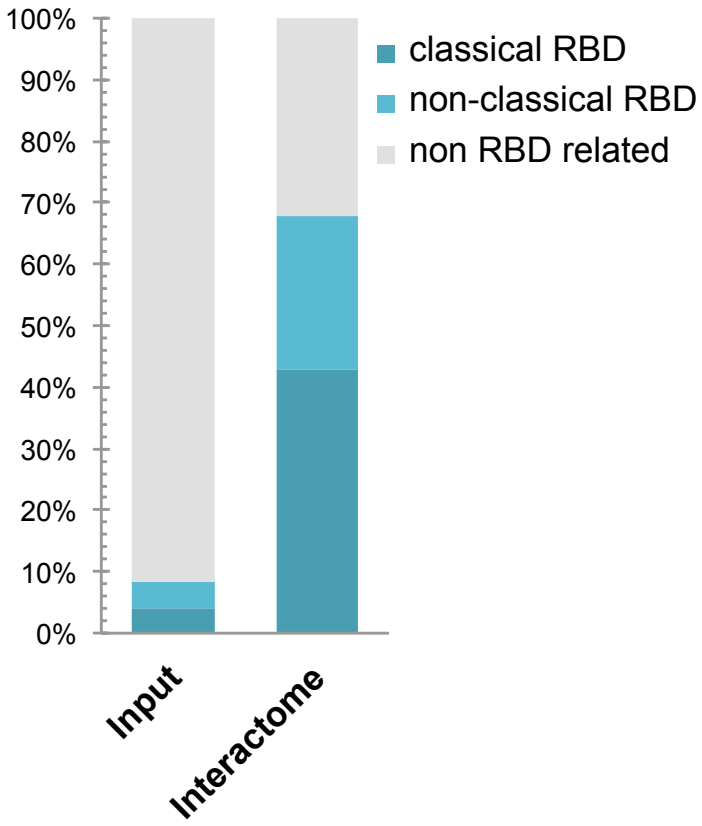

Supplemental Figure S4. Enrichment of proteins containing RNA-binding domains (RBD) in interactome capture. Proteins identified in the input and in the interactome capture were classified in three categories regarding the annotation of their Interpro domains as RBDs in Castello et al, 2012. If a protein contains a mixture of classical and non-classical domains, it is only counted once and only in the classical RBD category.

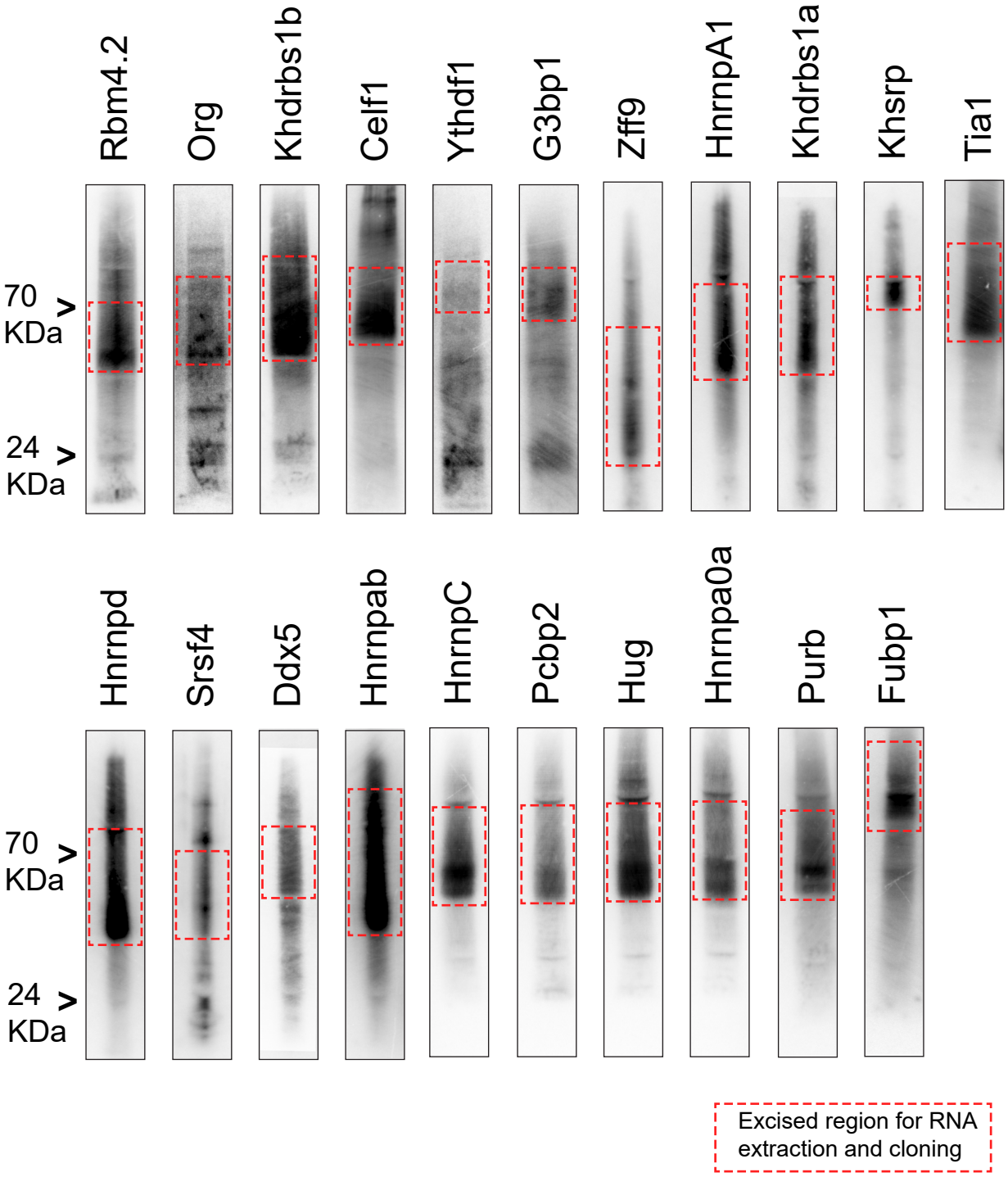

Supplemental Figure S5. Representative autoradiograms showing the localization of the ribo-protein complexes in a nitrocellulose membrane for iCLIP. The red dotted line indicates the region of the membrane that was cut and processed for RNA extraction and cloning.

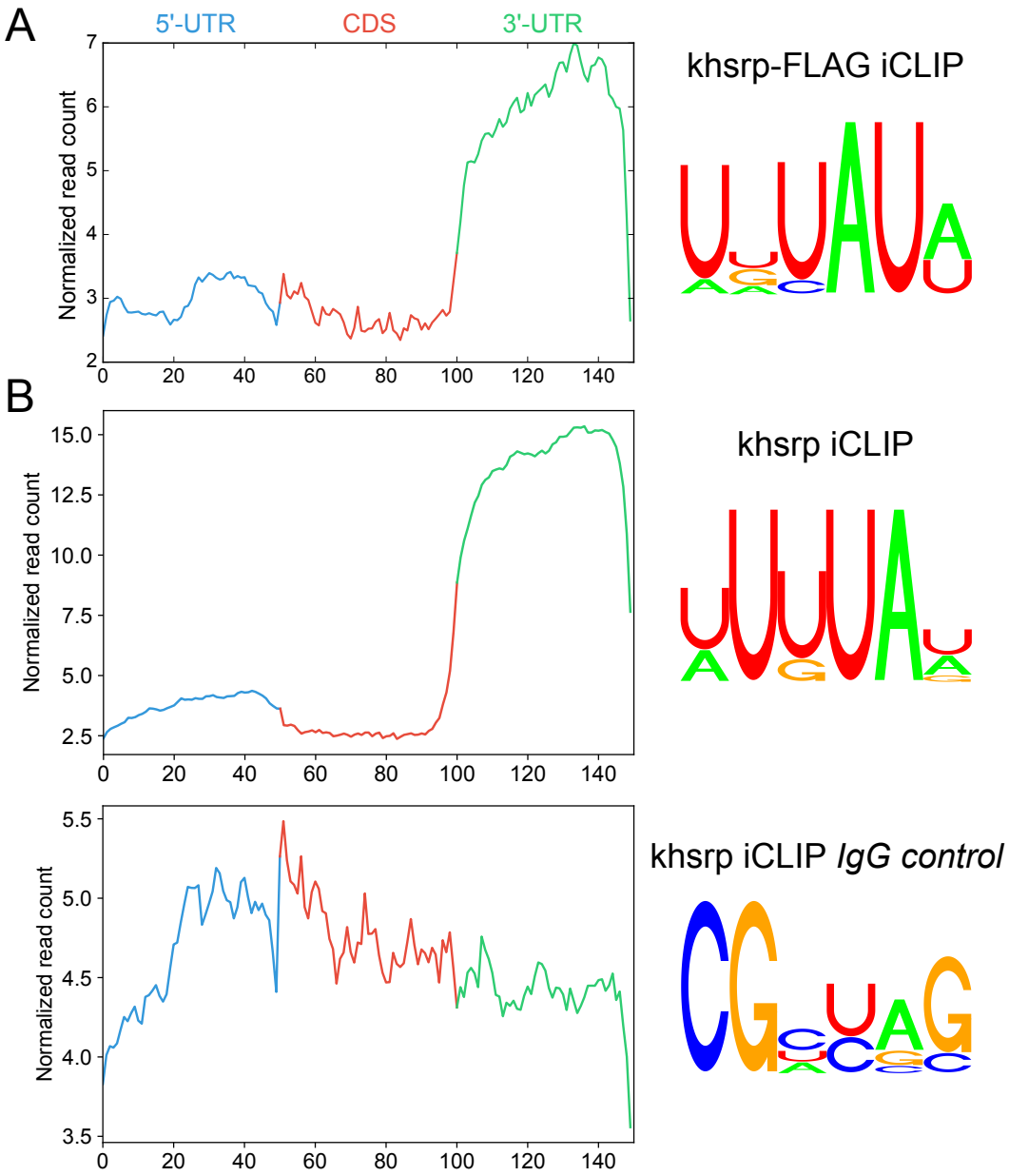

Supplemental Figure S6. Comparison of *khsrp* iCLIP with FLAG-tag (A) and endogenous (B) proteins. iCLIP metaplots of RBP-binding within protein-coding transcripts (left). Weblogo representation of the top 6-mer normalized by respective iCLIP control (right).

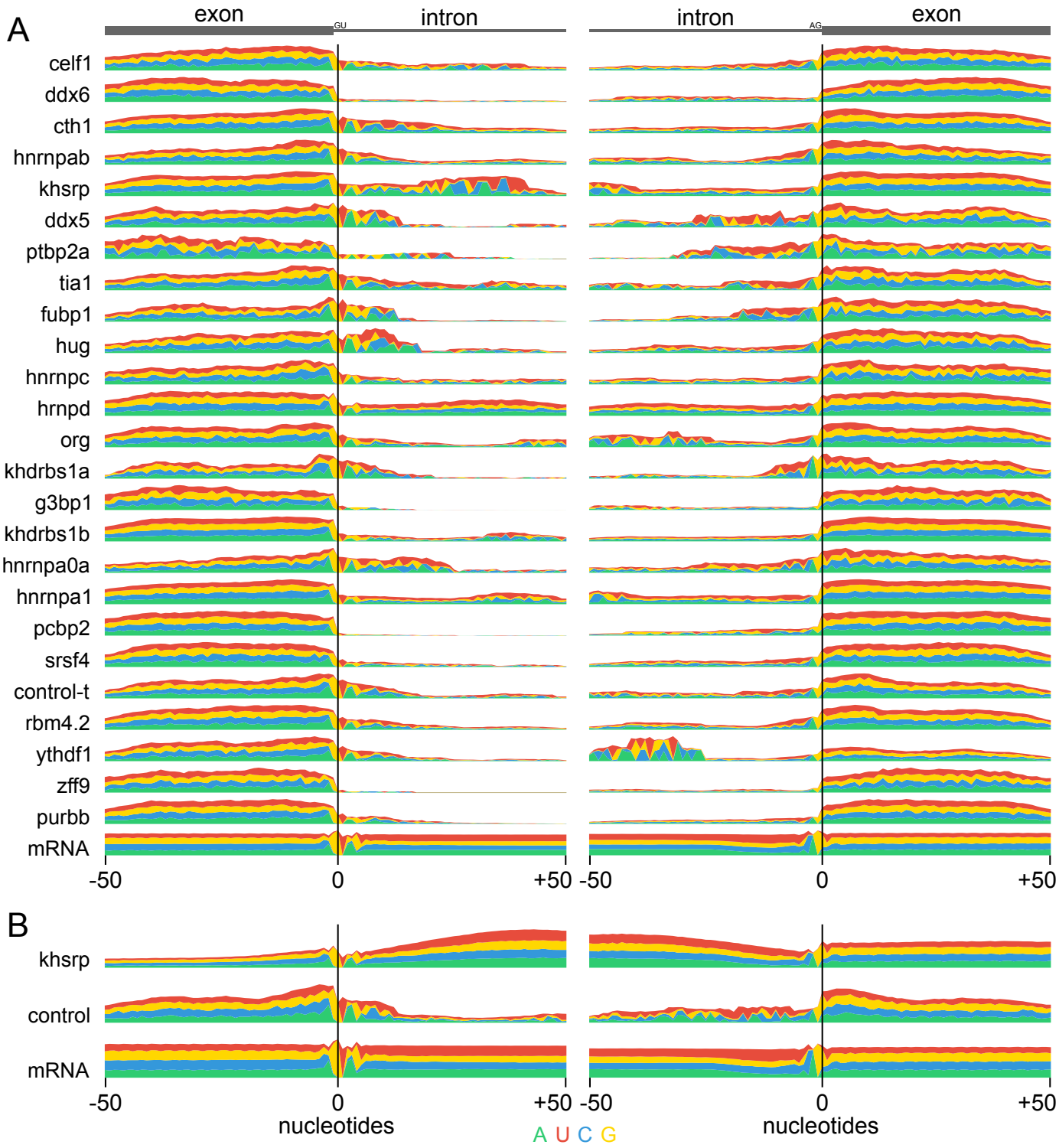

Supplemental Figure S7. Metaplots representing iCLIP read-coverage (normalized by library size) within a 100 nucleotide window at the exon junctions centered on the 5' donor (left) and the 3' acceptor (right) sites. RBP-binding signal was deconvoluted for each position into A (green), U (red), C (blue), and G (yellow) bases. Metaplot "mRNA" represents nucleotide bias at the exon-junction for all zebrafish transcripts. "control-t" is the top portion of the iCLIP control lane. RBP binding (A) for 24 iCLIP experiments and control from uninjected experiment, and (B) for *khsrp* iCLIP using endogenous antibody and control from no-antibody experiment.

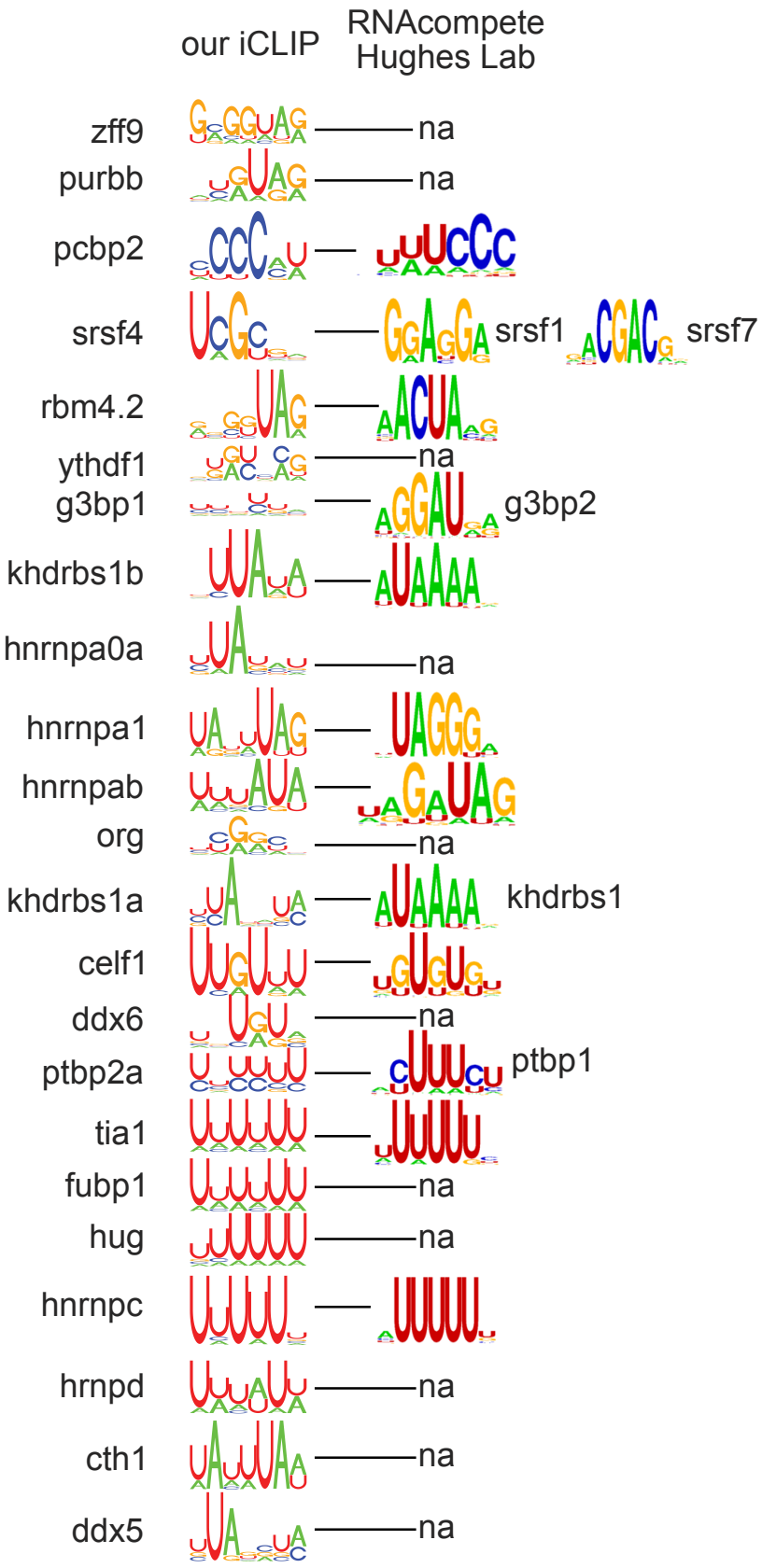

Supplemental Figure S8. Comparison of our iCLIP-derived motif with Ray et al, 2013 assay. When only a related protein was available, the name is shown. (na: not-available protein in Ray et al, 2013 database).

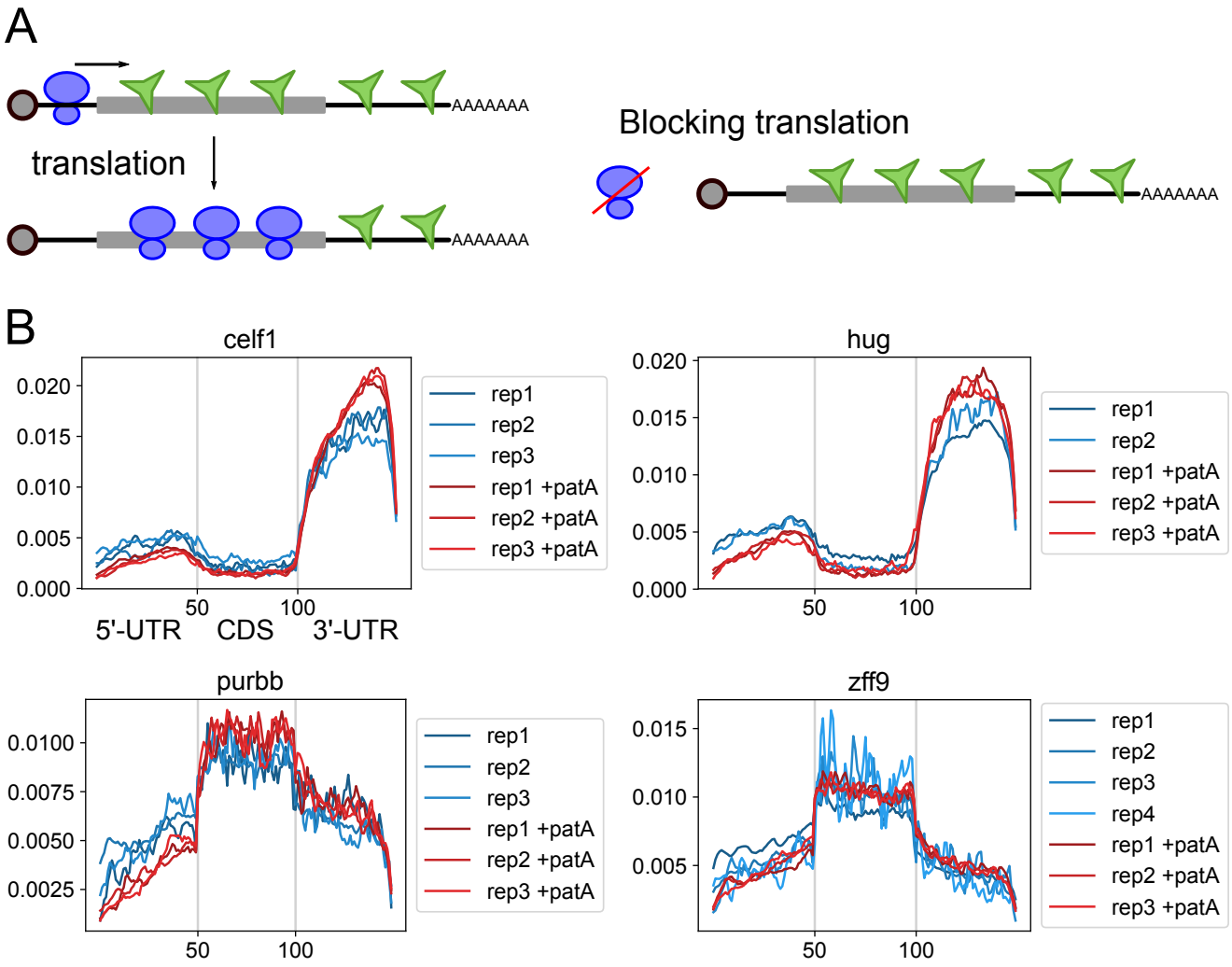

Supplemental Figure S9. Testing translation influence on RBP binding. The differential binding between coding and non-coding regions of RBPs could be induced by the translating ribosome preventing stable binding to the coding regions. Alternatively, the binding pattern might be determined by the preferential accumulation of binding motifs within those regions. To distinguish between these scenarios, translation was inhibited using pateamine A (patA), which prevents the formation of the translational initiation complex by inhibiting *eif4A*. Comparison of transcriptome metaplots for *celf1*, *hug*, *purbb*, and *zff9* in replicates in WT and patA treated embryos revealed similar enrichment in 3'-UTR regions after translation inhibition. (A) Diagram of hypothesis tested. Translating ribosomes that could actively push RBPs out of the coding-sequence would be blocked in presence of translation inhibitor patA. (B) iCLIP metaplots of RBP-binding within protein-coding transcripts comparing WT and patA treated embryos for *celf1*, *hug*, *purbb*, and *zff9* in replicates.

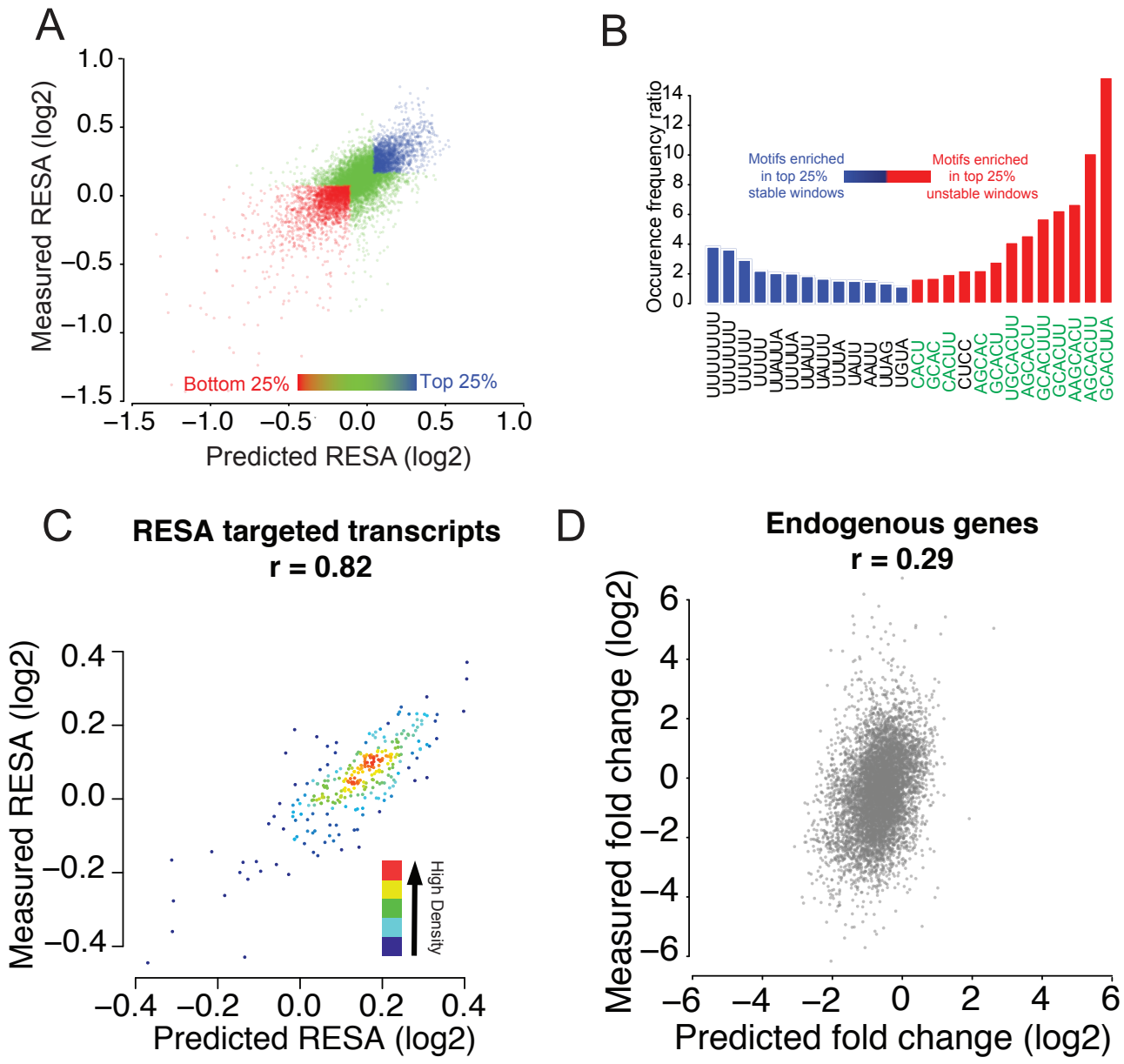

Supplemental Figure S10. RESA targeted random forest model. (A) Comparing mean motifs frequencies ratios in top 25% stabilizing and top 25% destabilizing windows (blue and red dots, respectively) against the middle control 50% windows (green dots) using model trained on RESA targeted library. (B) Motifs enriched in the top 25% stabilizing and top 25% destabilizing windows (blue and red bars, respectively). Y-axis represents per motif occurrence frequency ratio between top 25% stabilizing/destabilizing windows and middle 50% windows. All motifs selected have statistically significant *P* below 2.2×10^{-18} (Mann-Whitney *U* test followed by Bonferroni multiple testing adjustment). (C) Model (trained on RESA targeted library) performance per transcript using 5-fold cross validation. Model achieved a 0.82 Pearson correlation between mean predicted stability of all sliding windows across 3'-UTR of each transcript and mean measured stability from RESA profile of same transcript. Colors represent density (from red to dark blue, corresponding to high to low density, respectively). (D) Model (trained on RESA targeted library) performance on endogenous transcripts. Model achieved a 0.29 Pearson correlation between predicted fold-change measured as mean predicted stability of all windows across 3'-UTR and measured fold-change by poly(A) selected mRNA-seq.

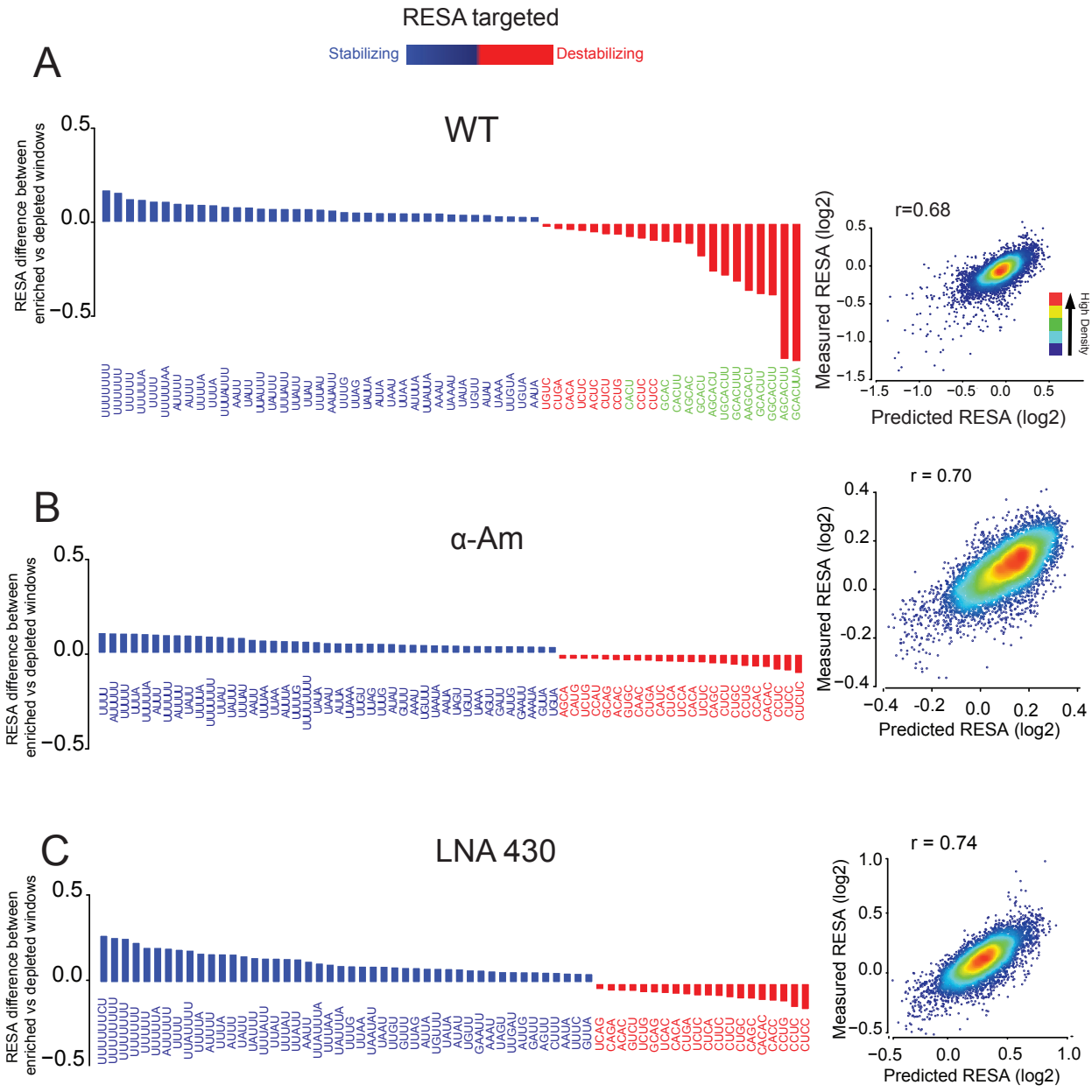

Supplemental Figure S11. Random forest-based motif selection for RESA targeted library. (A) (left) Top selected motifs according to the model trained on RESA targeted library. Y-axis represents the RESA fold-change difference between windows that do and do not contain each motif. All the motifs selected have statistically significant *P* below 4×10^{-42} (Mann-Whitney *U* test followed by Bonferroni multiple testing adjustment). Motifs in green text represent the miR-430 target sites. (right) Model performance per window using 5-fold cross validation; Model achieved a 0.68 Pearson correlation between predicted stability (x-axis) and measured stability (y-axis) according to RESA (colors represent density from red to dark blue, representing high to low density, respectively). (B) Same as (A), but the model was trained and tested after blocking transcription with an RNA polII inhibitor, α-amanitin. (C) Same as (A), but the model was trained and tested after miR-430 was inhibited using an antisense tiny-LNA complementary to miR-430 (LNA^{430}).

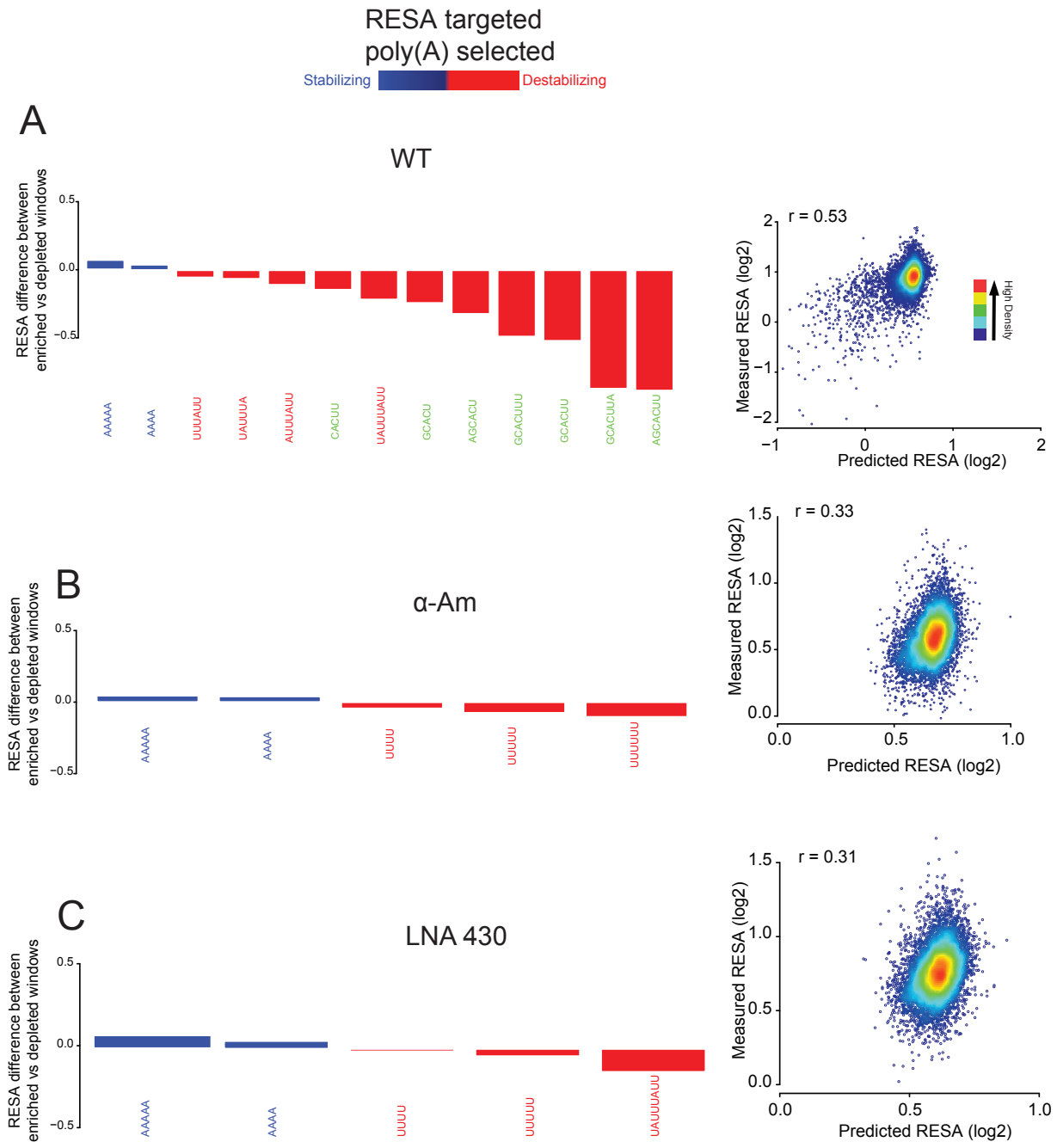

Supplemental Figure S12. Random forest based motif selection for RESA targeted with poly(A) selection library. (A) (left) Top selected motifs according to the trained model. Y-axis represents deadenylation difference between windows that do and do not contain each motif. All the motifs selected have statistically significant *P* below 0.01 (Mann-Whitney *U* test followed by Bonferroni multiple testing adjustment). Motifs in green text represent the miR-430 target sites. (right) Model performance per window using 5-fold cross validation. Model achieved a 0.53 Pearson correlation between predicted deadenylation (x-axis) and measured deadenylation according to RESA library (y-axis). Colors represent density (colors represent density from red to dark blue, representing high to low density, respectively). (B) Same as (A), but the model was trained and tested after blocking transcription with RNA polII inhibitor, α-amanitin. (C) Same as (A), but the model was trained and tested after miR-430 was inhibited using an antisense tiny-LNA complementary to miR-430 (LNA^{430}).

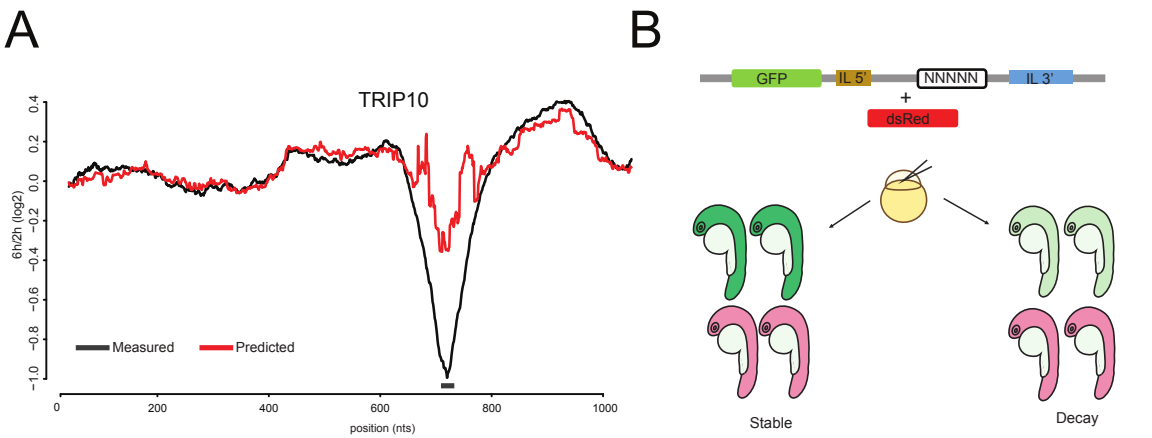

C

```
WT      AAATAATATAATTTATTGAGTAAATaagcgcttGTATATTAAATAAACATGTATGTAAGA
Mut1    AAATAATATAATTTATTGAGTAAATaaAAgGttGTATATTAAATAAACATGTATGTAAGA
Mut2    AcATAAcATcAcTcATcGAGTAAATaagcgcttGTATAccAcATAcACATGcATGTAAGA
Mut3    AcATAAcATcAcTcATcGAGTAAATaaAAgGttGTATAccAcATAcACATGcATGTAAGA
Mut4    AAgcAAgcTAgcTgcTTGAGgcAAgcaAAgGttGgcTATgcAAgcAACATGgcTGgcAGA
```

D

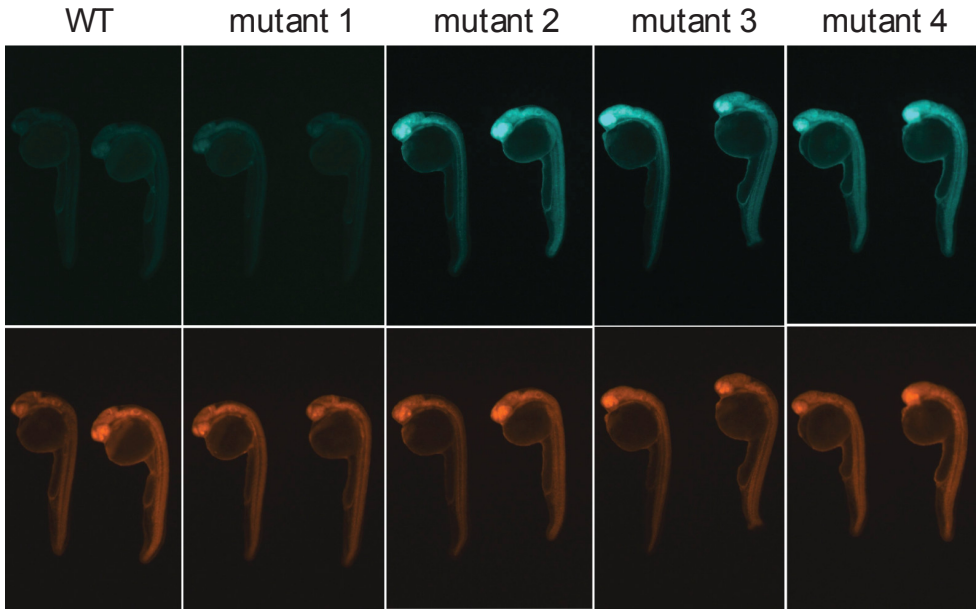

Supplemental Figure S13. *Trip10* transcript case study. (A) RESA targeted profile from the *trip10* locus comparing late/early fold-change (black curve) and predicted *trip10* profile using the random forest model (red curve) (B) Experimental design for validating the activity of injected mRNA reporters by comparing GFP levels to the control dsRed. (C) mRNA reporter sequences with miR-430 motif with a GU wobble and multiple AUUUA sequence motifs (green), and mutation introduced in each validation reporter (blue). (D) Assessment of the effect of each injected mRNA reporter on stability and protein output, by comparing dsRed control (bottom panel) and GFP (top panel) intensity to determine stability.

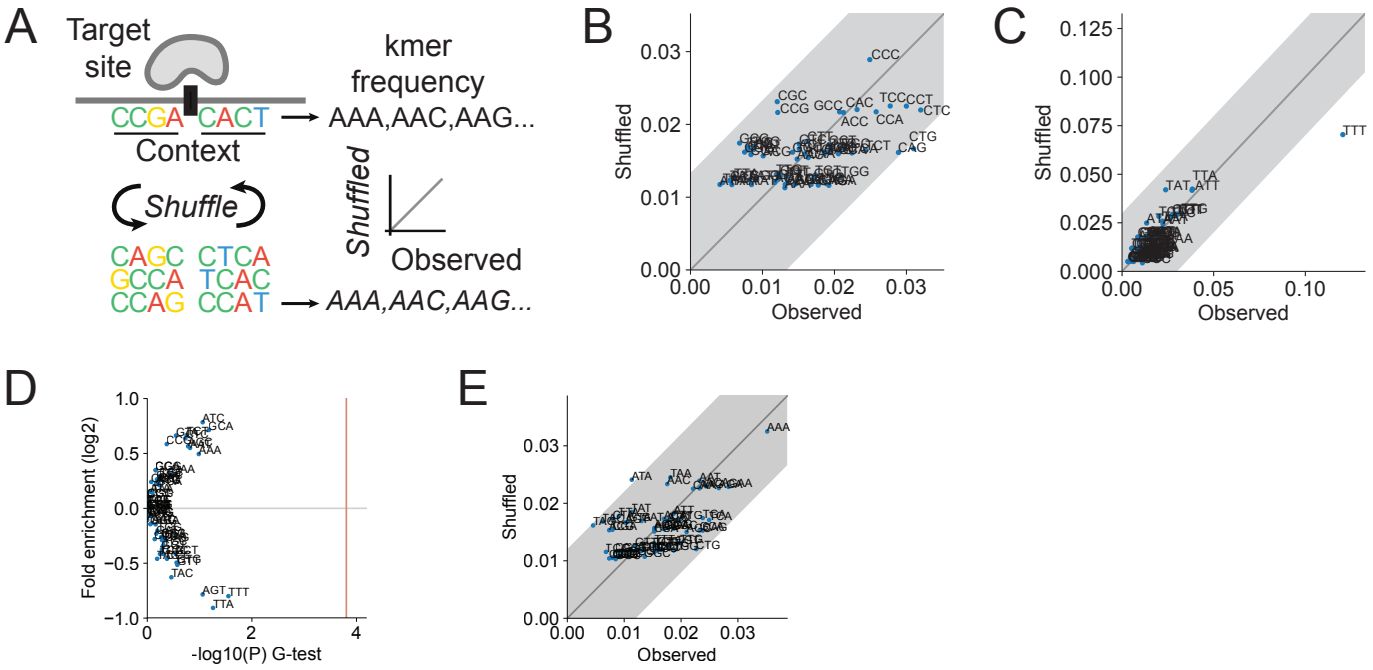

Supplemental Figure S14. Analysis to test if nucleotides are independent within target context. (A) Diagram showing the strategy used to determine if the context was preferentially enriched with specific motifs or limited to single nucleotides. Context sequences were shuffled while keeping the same nucleotide composition. (B) Similar motif frequency is shown between the observed and shuffled contexts, suggesting that the key feature of *pcbp2* binding context is nucleotide frequency. (C) For *hug*, the UUU 3-mer was enriched flanking *hug* binding sites compared to shuffled sequences, demonstrating a preference for adjacent Us in favorable *hug* binding, conferring stabilization. (D) Volcano plot representing 3-mer enrichment 20 nt upstream and downstream between the top 10% most destabilizing by miR-430 and the bottom 10%. *P* were calculated using G-test. Red line indicates 1% significance cutoff after Bonferroni multiple test correction. (E) Same as (B) for miR-430.